PCCP

Accepted Manuscript

ROYAL SOCIETY OF CHEMISTRY

www.rsc.org/pccp

Investigation of Molecular Partitioning Between Non Polar Oil Droplets and Aqueous Solution using Double Potential Step Chronoamperometry

Jonathan Newland, Patrick R. Unwin* and Julie V. Macpherson*

Department of Chemistry, University of Warwick, Coventry, CV4 7AL

Double potential step chronoamperometry (DPSC) is demonstrated as a technique for investigating partitioning between a solute in aqueous solution and non-polar oil droplet(s) immobilised at an electrode. Here a species in aqueous solution which does not partition into the oil phase is converted at the electrode surface into another species which either does not or does partition into the oil drop. The first case is investigated experimentally by considering generation of the ionic redox species, $FcTMA^{2+}$ from $FcTMA^{+}$, while the second case is exemplified by studies of Br_2 generation from Br^-. The case of molecular partitioning at the three phase interface has received little attention hitherto. To maintain oil droplet stability a boron-doped diamond electrode is employed functionalised with Pt nanoparticles to impart electrocatalytic activity on the electrode towards Br_2 production. An arrangement is utilised where the droplet(s) sit(s) on (but does not cover) the electrode surface. We show both experimentally and through finite element simulation how the charge-time profile for the generation and collection of electroactive species can be used to obtain information the extent of partitioning and how this is affected by factors such as the number and size of droplets. Finally, we highlight the suitability of this approach for investigating partitioning species induced reactions which take place within the droplet.

For submission to PCCP, January 2014; revised March 2014

Corresponding authors: **p.r.unwin@warwick.ac.uk; j.macpherson@warwick.ac.uk**

INTRODUCTION

The interface between two immiscible (liquid/liquid) interfaces is of fundamental interest to a range of chemical processes[1, 2]. Such an interface also serves as a simple model for biological membranes, allowing pharmacokinetic properties of drug/organic molecules, such as lipophilicity, to be determined.[3-5] Liquid/liquid interfaces play a critical role in many classes of chemical reactions, for example, phase transfer catalysis,[6-8] polymerization,[9] and substitution reactions, involving interfacial ion transfer (IT), electron transfer (ET) and/or molecular transfer.[10,11] As such, the electrochemical and phase transfer properties of liquid/liquid interfaces have been the subject of extensive study.[12] Significant research has focused on ion transfer between aqueous and organic phases,[13-17] with kinetics and mechanisms of two phase reactions determined via voltammetry[18] or microscale techniques such as scanning electrochemical microscopy (SECM)[19] and microelectrochemical measurements at expanding droplets (MEMED). [20, 21] The study of ET between two species at the interface of an oil droplet and an aqueous solution using laser trapping techniques has also been reported.[22]

Oil droplet modified electrodes represent an attractive format for the study of liquid/liquid interfaces, and also enable the study of ion transfer and photo-electrochemistry at three-phase junctions (solid-oil-water).[23-25] To date the vast majority of electrochemical studies with oil droplets have employed polar oils or oils that are redox active.[26] Non-polar oils have received less attention, partly due to the difficulty of incorporating a suitable electrolyte within them. Among a fairly limited body of work, uniformly-sized non-polar oil droplets decorating an electrode surface,[27] have been sized using single step potential-step chronoamperometry; an approach which can also be used to size other blocking materials[28].

In this paper, we demonstrate how double potential step chronoamperometry (DPSC) can be employed to probe the partitioning of an electrogenerated molecular species across the

non-polar oil (o) droplet/ aqueous solution (w) interface. Previous work has seen the use of SECM to directly measure molecular transport across this interface,[29] by using an ultramicroelectrode (UME), positioned in the aqueous phase (for example) to generate a molecular species, which is able to partition into the non-polar organic phase, during an initial potential step. Collection of the molecular species in a second step provides information on physicochemical parameters such as transfer kinetics and diffusion coefficient.[30]

Herein, we adapt this DPSC method for an arrangement where a droplet (or multiple droplets) sit(s) on, but does not completely cover, an electrode surface, immersed in electrolyte solution. We show how the current-time profile for the collection of the partitioning species - electrogenerated Br_2 (from Br^-) - depends not only on the size and number of droplet(s) on the electrode surface, but also on the time period of the generation step. The DPSC responses are also compared to those for a system where no partitioning occurs at the o/w interface, i.e. for an ionic redox couple. The potential advantage of this approach compared to SECM is a greatly simplified experimental arrangement, negating, for example, the need for tip positioning.

EXPERIMENTAL

Chemicals: Potassium bromide, 99.5% (Fisons Scientific Equipment, UK), 0.5 M sulfuric acid solutions diluted from 18 M sulfuric acid (VWR international Ltd. UK), ferrocene tetramethylammonium ($FcTMA^+$) hexafluorophosphate (produced in house via the metathesis of the corresponding iodide salt (99%, Strem) with ammonium hexafluorophosphate (99.5%, Strem)[31]) and dodecane (Sigma Aldrich, UK) were used herein. All aqueous solutions were made using 18.2 MΩ cm (25 ºC) Milli-Q filtered water (Millipore Corporation).

Instrumentation and protocols: Negligible sp^2 content, polycrystalline boron doped diamond (pBDD) 1 mm diameter, macrodisc electrodes[32] were prepared in house using a reported procedure,[33] from DIAFILM EA grade pBDD (supplied in wafer form by Element Six, Harwell; average boron dopant density ~ 3×10^{20} B atoms cm^{-3} and lapped to produce a surface roughness ~ nm[34]). pBDD was employed as the electrode material to circumvent possible problems due to the reported instability of organic droplets on some metal electrodes under potential control.[35] As the Br^-/Br_2 heterogeneous redox process is sluggish on bare pBDD (*vide infra*) functionalisation of the pBDD substrate with Pt nanoparticles (NPs) was necessary. Pt NPs, 20-40 nm in size, were formed at the pBDD surface by electrodeposition from a solution containing 1 mM K_2PtCl_6 and 0.1 M HCl. The pBDD electrode was held at a potential of -1.0 V vs. a saturated calomel electrode (SCE) for 5 s, using a reported procedure[33]. Prior to oil droplet deposition, any Pt oxide present on the surface of the NPs was electrochemically reduced by holding the electrode at -1 V in a solution of 0.5 M sulfuric acid, for 40 s. This optimized the Pt NP-pBDD electrode towards the Br^-/Br_2 couple

The Pt NP-pBDD electrode was mounted vertically, facing upwards, in a 4 cm diameter Teflon cell base and secured in place with paraffin wax. The cell was completed by placing a glass cell body, containing a 2 cm diameter quartz window (for microscopy visualization), over the cell base, held in place with a rubber O-ring. The cell was filled with the solution of interest and electrochemical analysis was carried out using a CH Instruments Electrochemical Analyzer, model CHI 1105A (CH instruments, Austin, Texas, USA), in a 3-electrode mode, with a Pt wire counter electrode. All potentials are quoted versus SCE, which was employed as the reference electrode (BAS Inc., Tokyo, Japan). Measurements were made at room temperature (22 ± 1 ºC).

Dodecane oil droplets, typically in the size range 100 – 1450 μm diameter, were deposited on the surface of the Pt NP – pBDD electrode using 30-40 μm o.d. tapered borosilicate

pipettes, pulled from 2 mm o.d, 1.16 mm i.d borosilicate tubes (Harvard Apparatus) using a pipette puller. The pipette was mounted on a manual micro-positioner (M433 series, Newport) which was capable of movement in the *x*, *y* and *z* directions, with micron resolution. Oil droplets were dispensed by applying pressure to the oil filled pipette using a 5 mL syringe (BD Plastipak) with the size controlled by the period of time for which the pressure was applied. The sizes of the oil droplets were determined optically, *in-situ*, using two PixeLINK (Ottawa, Canada), 3-megapixel cameras, one positioned above the electrode (top view), and the other to the side facing the quartz window (side view). The top camera was fitted with a 4× telecentric lens (Edmund optics, model 62763) or 2× telecentric lens (Infinistix), while the side camera was fitted with a 2× telecentric lens (Infinistix). Illumination was provided by a Fiber-Lite DC-950 regulated illuminator (Dolan-Jenner Industries).

The partition coefficient (K) of Br_2 between dodecane and water, at room temperature, was determined by recording the UV-Visible absorption (Cary 50 Bio UV-Visible spectrophotometer) spectrum (peak maximum for Br_2, A_{max}, at 393 nm) of aqueous 20 mM Br_2 (Fisher Scientific), before and after mixing thoroughly with an equal volume of dodecane, for 30 s. Longer mixing times were found to have no difference on the absorbance spectra recorded. We found K = 10.6 ± 0.7 (1σ) at room temperature (22 ± 1 ^{o}C). For comparison, K was also determined using voltammetry on a 2 mm diameter Pt macrodisc electrode where the potential was swept from +1 V to +0.5 V (vs. SCE), scan rate 0.1 Vs^{-1}, in a solution of 20 mM $Br_{2\ (aq)}$ before and after shaking with an equal volume of dodecane, we obtained K = 9.3 ± 1.1 (1σ) at room temperature, consistent with absorbance measurements.

SIMULATIONS

Simulations were performed on a Dell Optiplex 755, Intel Core 2 Quad 2.49 GHz computer equipped with 8 GB RAM running windows XP 64 bit edition. Comsol Multiphysics 4.2 (Comsol AB, Sweden) was used for finite element modeling. Simulations employed a minimum of 64,000 triangular mesh elements. The highest mesh resolution was focused around the electrode surface and o/w interfaces.

We consider a macroelectrode immersed in an aqueous electrolyte solution (phase w) supporting a droplet of dodecane (phase o) centred on the electrode surface, shown in Figure 1 (a). During a typical DPSC experiment, in the forward step a potential is applied for a fixed amount of time, τ, sufficient to generate B via the electrooxidation of A in solution, at a diffusion-controlled rate, *i.e.*;

$$m\mathrm{A} \rightarrow \mathrm{B} + ne^- \qquad (1)$$

where n is the number of electrons transferred per mole of reactant, m is the stoichiometry of A. In the reverse step a potential is applied, for a further time, τ (total duration of experiment 2τ), sufficient to collect B via electroreduction to A in accordance with;

$$\mathrm{B} + ne^- \rightarrow m\mathrm{A} \qquad (2)$$

at a diffusion-controlled rate.

We consider two situations: (1) Where neither A nor B interacts with or partitions across the o/w interface, and (2) where A does not partition, but B does according to:[36]

$$\frac{[B_{(org)}]}{[B_{(aq)}]} = K \qquad (3)$$

The diffusion of species A and B is described by the following time-dependent diffusion equation and solved for the simulated axisymmetric cylindrical geometry formed from a 2D domain, shown in Figure 1 (a).

$$\frac{\partial c_j}{\partial t} = D_j\left(\frac{\partial^2 c_j}{\partial r^2} + \frac{1}{r}\frac{\partial c_j}{\partial r} + \frac{\partial^2 c_j}{\partial z^2}\right) \qquad (4)$$

where c_j is the concentration of species A or B (mol cm^{-3}), D_j is the diffusion coefficient of a species A or B (cm^2 s^{-1}), z is the coordinate normal to the electrode surface (cm), r is the radial coordinate (cm) and t is time (s).

The boundary conditions listed in Table 1 were applied to create a model of the DPSC system. During the forward step (electrogeneration of redox species B from A), the concentration of A at the electrode boundary was set to c = 0. The outward flux of B at the electrode boundary was dependent on the inward flux of A and was set with mA → B, where m is 1 for $FcTMA^+/FcTMA^{2+}$ and 2 for Br^-/Br_2.

The model considered oil droplets of various sizes supported on the electrode surface. The droplet shape, including diameter and contact angle, were determined from optical images.. The diffusion coefficients for Br_2 and the Br^- ion in aqueous solution used in the model were taken from previous studies;[25] $D_{Br^-\,(aq)} = 1.85 \times 10^{-5}$ cm^2 s^{-1} and $D_{Br_2\,(aq)} = 9.4 \times 10^{-6}$ cm^2 s^{-1}. For Br_2 transport across the w/o interface, a fast mass transfer coefficient, k_1 of 0.5 cm s^{-1} is assumed, which corresponds to a diffusion-controlled situation under the experimental conditions. A mass transfer coefficient, k_{-1} of 0.05 cm s^{-1} is implied for the reverse movement of Br_2 across the o/w interface, given K = 10. For the concentration of Br^- employed (and Br_2 produced) we can reasonably ignore the formation of Br_3^-.[37] The diffusion coefficient for both $FcTMA^+$ and $FcTMA^{2+}$ was 7.6×10^{-6} cm^2 s^{-1}.[38]

To investigate how the DPSC response for the Br^-/Br_2 system varied when employing arrays of oil microdroplets, simulations of homogeneously sized arrays, of spacing d = 100 μm, were performed with a time pulse, τ, of 2 s. Array simulations utilized a diffusion domain approach, with an axial symmetric domain representing the electrode surface and bulk solution[23], (see Figure 1(b)) using the boundary conditions described in Table 2. The macroelectrode current is calculated from the flux of A_1 at the electrode surface.

DPSC Experiments

Two systems are considered herein: the fast ET, outer sphere redox species, **FcTMA$^{+/2+}$** where A = FcTMA^{+}, B = FcTMA^{2+}, n = 1, and **Br^{-}/Br$_2$** where A = Br^{-}, B = Br$_2$, n = 2. For DPSC with FcTMA$^{+/2+}$ in the forward step a potential of +0.6 V was applied of pulse width τ, whilst a potential of +0.15 V was applied, during the reverse step, for equal τ.

For the Br^{-}/Br$_2$ redox couple, DPSC experiments were performed by applying an open circuit potential to the electrode for 120 s (allowing the system to stabilize between experiments) before holding at +1.2 V versus SCE (the forward step) for time, τ. The potential was then switched to +0.7 V (reverse step).

RESULTS and DISCUSSION

As shown in Figure 2, the use of Pt NPs makes Br^{-}/Br$_2$ electrolysis more kinetically facile[39] (red dotted line), compared to pBDD alone (black line), while retaining the inherent low background currents of pBDD electrodes.[40] The density of Pt NPs is also sufficient that on the timescale of the cyclic voltammogram (CV) there is complete diffusional overlap and the response is comparable to that of a Pt macroelectrode (black dotted line). Importantly, the presence of Pt NPs on the electrode surface (see Figure 2b) does not lead to any destabilization of oil droplets on the electrode surface over the applied potential range.

Effect of droplet size: Charge-time (Q-t) responses of the FcTMA$^{+/2+}$ system were investigated experimentally for the Pt NP-pBDD electrode in the absence (black line) and presence of a single dodecane oil droplet, in the size range d = 100 μm (■), 200 μm (▲) and 400 μm (▼), as shown in Figure 3a. When comparing the DPSC responses, the presence of an oil droplet can be seen to diminish the current, and hence charge (Q) response, for the generation step. In general the larger the droplet, the lower the Q passed (Figure 3a). This is

clearly because the droplet blocks part of the electrode and hinders diffusion to part of the electrode near the droplet. By normalizing Q with respect to the maximum Q i.e. Q/Q_{max} (at τ = 2 s), the amount of species collected back can be compared to the total amount generated during the forward step (Figure 3b).

Close inspection of the plot of Q/Q_{max} vs. t at long times reveals that in the presence of the oil drop the amount of charge collected back, relative to the amount of charge generated in the forward step is always greater than that at a bare electrode surface (i.e. lower Q/Q_{max}; the current passed during generation is in the opposite direction to that passed during collection). Second, this effect is exacerbated the larger the oil drop as diffusion of the electrogenerated species, $FcTMA^{2+}$, away from the electrode is hindered compared to the bare electrode case, due to the presence of the oil drop. This is shown clearly by the FEM-generated concentration profiles for $FcTMA^{+/2+}$ generation/collection for droplets of 100 μm diameter (Figure 3ci) and 400 μm diameter (Figure 3cii) at τ = 2 s and 2τ. As the droplet size increases a greater proportion of $FcTMA^{2+}$ is "trapped" by the inert droplet, so that more is available locally for collection during the reverse potential step.

Figure 4a shows Q-t transients (τ = 2 s), for the Br^-/Br_2 system, for a bare electrode surface (black line) and a surface covered with a single dodecane oil droplet, with d in the range 100 μm (■), 200 μm (▲), 400 μm (▼) 1000 μm (◀) and 1450 μm (♦). Optical images of the dodecane droplets are shown in Figures 3d and 4b. As for $FcTMA^{2+}$ generation, during the forward step as the size of the droplet increases, blocking the electrode, the amount of Br_2 generated (i.e. Q) decreases. In contrast to Figure 3b, however, the amount of Br_2 collected back, relative to the amount initially generated, is less than for a bare electrode surface (*i.e.* higher Q/Q_{max} values are seen at all times) and decreases with increasing droplet size (Figure 4c). This effect can be attributed to partitioning of the electrogenerated Br_2 from the aqueous phase into the non-polar oil droplet, thereby removing Br_2 from the electrochemically

accessible region of the electrode during the collection step. For the largest droplet studied (d = 1450 μm) the Q/Q_{max} response tends towards 1, where 1 denotes no Br_2 collected back.

To explain the trend seen experimentally, Figure 5 shows simulated Br_2 concentration profiles at τ (t = 2 s) and 2τ for single (a) 100 μm and (b) 400 μm diameter droplets on an electrode. At the end of the forward potential step, the diffusion of electrogenerated Br_2 away from the electrode surface and into the oil phase can clearly be seen. For the case of the 100 μm diameter droplet and τ = 2 s, the relatively higher interfacial area to volume ratio results in the oil droplet containing a significantly higher concentration of Br_2 than the 400 μm diameter droplet.

During the collection step, Br_2 is depleted at the electrode surface in the aqueous solution, resulting in oil-phase partitioned Br_2 being released into the aqueous solution for subsequent collection. For the small drop, the efficient trapping of Br_2 results in a high Br_2 collection efficiency. For larger droplets, the droplet actually provides an escape route away from the electrode with some Br_2 diffusing out of the drop into solution regions where collection cannot occur resulting in less Br_2 collected back and thus higher Q/Q_{max} values, at $t > \tau$.

Figure 6 presents the simulated DPSC response (Figure 6a), plotted as Q/Q_{max} vs. t for the collection step, alongside that observed experimentally (Figure 6b) for droplets of 100 μm, 200 μm and 400 μm diameter. Qualitatively, the simulated and experimental data show the same trend of decreasing Br_2 collection with increasing droplet size. There is a discrepancy between experiment and simulation, which could be due to subtle differences in the droplet shape in the model and experiments and/or natural convection effects, particularly in the larger droplets and at longer times, which is not taken into account in the simple diffusion simulations.

Effect of τ. The effect of τ on the Q/Q_{max} - t response for Br^-/Br_2 was investigated experimentally over the τ range 200 ms - 20 s. We focused on analysis of the reverse step as this informs on the partitioning process, i.e. we analyse data at $t \geq \tau$. Relatively small droplets were employed. Figure 7 shows Q/Q_{max} - t responses for both the bare electrode and one containing a single oil drop of d = 100 µm (●) and 200 µm (▲). In general, as τ increases, more of the o/w interface becomes accessible to the expanding diffusion field of electrogenerated Br_2, resulting in a decrease in the amount of Br_2 collected back (higher Q/Q_{max} value) for the reasons outlined above. Interestingly, for the shortest pulse times investigated (τ = 200 ms and 1 s) (Figures 7a,b), very little difference was seen in the normalised Br_2 collection responses for droplets that were 100 and 200 µm in diameter. However, as τ increased, the impact of Br_2 partitioning could be more easily differentiated (e.g. Figure 7c for τ = 10 s). As τ increased further, this differentiation increased (Figure 7d).

Effect of electrode size: To complement the studies above, we carried out further simulations keeping the droplet size constant at 100 µm (red symbols) and 200 µm (blue symbols) diameters but with different support electrode diameters of 100 µm (●), 200 µm (▲), 300 µm (▼) and 500 µm (■). These data are shown in Figure 8, (Q/Q_{max} versus t) for τ = 200 ms along with the bare electrode response (black line). It can be seen that as the electrode size approaches that of the oil droplet the difference between the collection responses for 100 µm and 200 µm diameter droplets increases enabling differentiation and sizing. These data further illustrate that one can tune the relative sizes of electrode and droplet, as well as the pulse time in DPSC to maximise the sensitivity with which the droplet can be sized and/or partitioning probed.

Non-spherical droplets: The contact area of an oil droplet with the surface of an electrode can have a pronounced effect on the collection response. In Figure 9a, two oil droplets, d ~ 1000 µm (i ■) and 1700 µm (ii ●), where d is measured across the center of the

droplet, have similar contact areas with the electrode surface but different droplet geometries. This is emphasized by optical images (Figure 9a) taken from above the electrode surface with a side light to define areas where contact between the dodecane oil and modified-diamond surface occurs (right hand side images). These larger droplets were deposited by addition of dodecane oil to the top of droplets pre-deposited on the electrode surface.

The generation and collection responses for $\tau = 2$ s for these two droplets (Figure 9b) are very similar, making it difficult to distinguish between them, even though the geometries are very different. In contrast, for two larger droplets of $d \sim 2500$ µm (iii ▲) and 3000 µm (iv ▼), which again have similar contact areas with the electrode, there is now a clear difference in the current collection response. For the bigger droplet more Br_2 is collected back compared to the smaller droplet, in contrast to the trend observed for spherical droplets in Figure 4c. This is due to the significantly distorted shape of the $d \sim 3000$ µm droplet a product of the buoyancy of the dodecane oil resulting in a "balloon" like construct, effectively pulling the oil droplet away from the electrode surface. As the o/w interface is pulled away from the electrode surface, Br_2 partitioning into the oil droplet is less efficient and as a result, more Br_2 is collected back in the reverse potential step. This brief analysis highlights the care that needs to be taken in analyzing the charge (current) response if DPSC is to be used for accurate oil droplet sizing.

Droplet arrays: We finally consider the impact of multiple droplets on an electrode surface. An array of twenty-one dodecane oil microdroplets ($d \sim 100$ µm) were created on the surface of a Pt NP-pBDD electrode and submerged in a solution of 10 mM KBr, 0.5 M H_2SO_4; Figure 10a. DPSC was performed on the droplet array ($\tau = 2$ s). Normalized Q/Q_{max} -t plots are shown in Figure 10b for the bare electrode surface (black line), a single droplet (d = 100 µm: ■) and the array of droplets (d = 100 µm: ▲)with an approximate spacing of ~ 170 µm (centre to centre). Crucially, compared to the bare electrode and the electrode

functionalized with one oil droplet, significantly less Br_2 is collected back, because of the enhanced trapping of Br_2 by multiple droplets. Figure 10c shows the FEM-simulated Br_2 concentration profile for a small section of the droplet array, at $\tau = 2$ s (Br_2 generation step) created by stitching together multiple concentration profiles generated from the diffusion domain in Figure 1b. It can be seen that the majority of the o/w interface of each droplet sits well within the electrogenerated Br_2 diffusion field.

CONCLUSIONS

DPSC has demonstrated sensitivity towards the sizing of non-polar oil droplets on an electrode surface, in aqueous solution. The importance of the interaction between the electrogenerated species and the oil droplet has been highlighted by DPSC responses on different sized dodecane droplets with both a partitioning electrogenerated species, i.e. Br_2, and a non-partitioning electrogenerated species, i.e. $FcTMA^{2+}$. The amount of charge collected back, relative to the amount of charge generated in the forward step, is always greater than that at a bare electrode surface for the non-partitioning species and less than that at a bare electrode for the partitioning species. DPSC can thus provide a facile approach to examining the extent of partitioning of an electrogenerated species.

Focusing on the partitioning species, key factors which influence the *Q-t* response and cause it to vary from that at a bare electrode have been identified. First, the oil droplet size and o/w interface/volume ratio is important. DPSC analysis of dodecane oil microdroplets combined with simulation data has emphasized how the size of the diffusion field (normal to the electrode) during the generation step in relation to the size of the oil droplet impacts the *Q-t* response. Droplets sitting within the generated diffusion field trap Br_2 which can be collected back at the electrode surface. In contrast, droplets which have significant portions lying outside the field provide a route by which Br_2 can escape detection in the collection

step. For most efficient collection, the diffusion field should be of similar size or smaller than that of the oil droplet. The diffusion field size is controlled by τ. Second, the size of the electrode relative to that of the oil droplet is significant. As the size of the electrode approaches that of droplet, the amount of Br_2 collected back becomes significantly lower than that for a bare electrode alone. Finally, microdroplet arrays enhance the sensitivity of the overall approach. For future work, we envisage the use of DPSC to monitor reactions taking place within a droplet and also for probing partitioning at modified o/w interfaces.

ACKNOWLEDGEMENTS

The authors would like to thank EPSRC and BP for the award of a CASE studentship to JN, Element 6 for providing the diamond material and Drs. Kate Meadows, Massimo Peruffo and Maxim Joseph (Department of Chemistry, University of Warwick) for helpful discussions.

Table.1: Boundary conditions for the finite element model where **n** is the inward-pointing unit normal vector; N is the normal flux of species; species A_w is A in the aqueous phase, species B_w is B in the aqueous phase and B_w is B in the oil phase (Br^-/Br_2 system only), with the subscript denoting the phase occupied by the species; k_1 and k_{-1} are the mass transfer coefficients equal to 0.5 cms^{-1} and 0.05 cm^{-1} respectively, D_j is the diffusion coefficient of a given species j where j = A or B. When considering the Br^-/Br_2 system, for species A_w, $D = 1.85 \times 10^{-5}$ cm^2 s^{-1}; species B_w and B_o, $D = 9.4 \times 10^{-6}$ $cm^2 s^{-1}$. For the $FcTMA^{+/2+}$ system, for both species A_w and B_w, $D = 7.6 \times 10^{-6}$ cm^2 s^{-1}.

Edge Number	*Physical representation*	*Boundary Conditions*
1	Axial symmetry	$-\mathbf{n}\cdot N_{B_o} = 0$
2	Blocked electrode	$-\mathbf{n}\cdot N_{A_w} = 0$ $-\mathbf{n}\cdot N_{B_o} = 0$
3	Axial symmetry	$-\mathbf{n}\cdot N_{A_w} = 0$ $-\mathbf{n}\cdot N_{B_w} = 0$
4	Electrode surface	$0 \le t \le \tau$, $c_{A_w} = 0$ $0 \le t \le \tau$, $-\mathbf{n}\cdot N_{B_w} = \frac{1}{n}(D_{A_w}\nabla C_{A_w})$ $t > \tau$, $-\mathbf{n}\cdot N_{A_w} = n(D_{B_w}\nabla C_{B_w})$ $t > \tau$, $c_{B_w} = 0$ $n = 1$ ($FcTMA^{+/2+}$) $n = 2$ (Br^-/Br_2)
5	Glass insulation	$-\mathbf{n}\cdot N_{A_w} = 0$ $-\mathbf{n}\cdot N_{B_w} = 0$
6/8	Bulk solution	$c = c^*$
7/9	Oil/water interface	$-\mathbf{n}\cdot N_{A_w} = 0$ $-\mathbf{n}\cdot N_{B_w} = 0$ ($FcTMA^{+/2+}$) $-\mathbf{n}\cdot N_{B_w} = -k_1 c_{B_w}$ $-\mathbf{n}\cdot N_{B_w} = (k_{-1})c_{B_o}$ $-\mathbf{n}\cdot N_{B_o} = -(k_{-1})c_{B_o}$ $-\mathbf{n}\cdot N_{B_o} = k_1 c_{B_w}$

Table.2: Boundary conditions for droplet array finite element model where **n** is the inward-pointing unit normal vector; N is the normal flux of species; species A_w is A in the aqueous phase, species B_w is B in the aqueous phase and B_o, B in the oil phase (Br^-/Br_2 system only), with the subscript denoting the phase occupied by the species; k_1 *and* k_{-1} are the mass transfer coefficients equal to 0.5 cm s^{-1} and 0.05 cm s^{-1} respectively, D_j is the diffusion coefficient of a given species (A or B). When considering the Br^-/Br_2 system, for species A_w, $D = 1.85 \times 10^{-5}$ cm^2 s^{-1}; species B_w and B_o, $D = 9.4 \times 10^{-6}$ cm^2 s^{-1}.

Edge Number	*Physical representation*	*Boundary Conditions*
1	Axial symmetry	$-\mathbf{n}\cdot N_{B_o} = 0$
2	Axial symmetry	$-\mathbf{n}\cdot N_{A_w} = 0$
		$-\mathbf{n}\cdot N_{B_w} = 0$
3	Blocked electrode	$-\mathbf{n}\cdot N_{A_w} = 0$
		$-\mathbf{n}\cdot N_{B_o} = 0$
4	Electrode surface	$0 \le t \le \tau$, $c_{A_w} = 0$
		$0 \le t \le \tau$, $-\mathbf{n}\cdot N_{B_w} = \frac{1}{2}(D_{A_w}\nabla c_{A_w})$
		$t > \tau$, $-\mathbf{n}\cdot N_{A_w} = 2(D_{B_w}\nabla c_{B_w})$
		$t > \tau$, $c_{B_w} = 0$
5	Reflective boundary	$-\mathbf{n}\cdot N_{A_w} = 0$
		$-\mathbf{n}\cdot N_{B_w} = 0$
6	Bulk solution	$c = c^*$
7/8	Oil/water interface	$-\mathbf{n}\cdot N_{A_w} = 0$
		$-\mathbf{n}\cdot N_{B_w} = -k_1 c_{B_w}$
		$-\mathbf{n}\cdot N_{B_w} = (k_{-1})c_{B_o}$
		$-\mathbf{n}\cdot N_{B_o} = -(k_{-1})c_{B_o}$
		$-\mathbf{n}\cdot N_{B_o} = k_1 c_{B_w}$

FIGURES

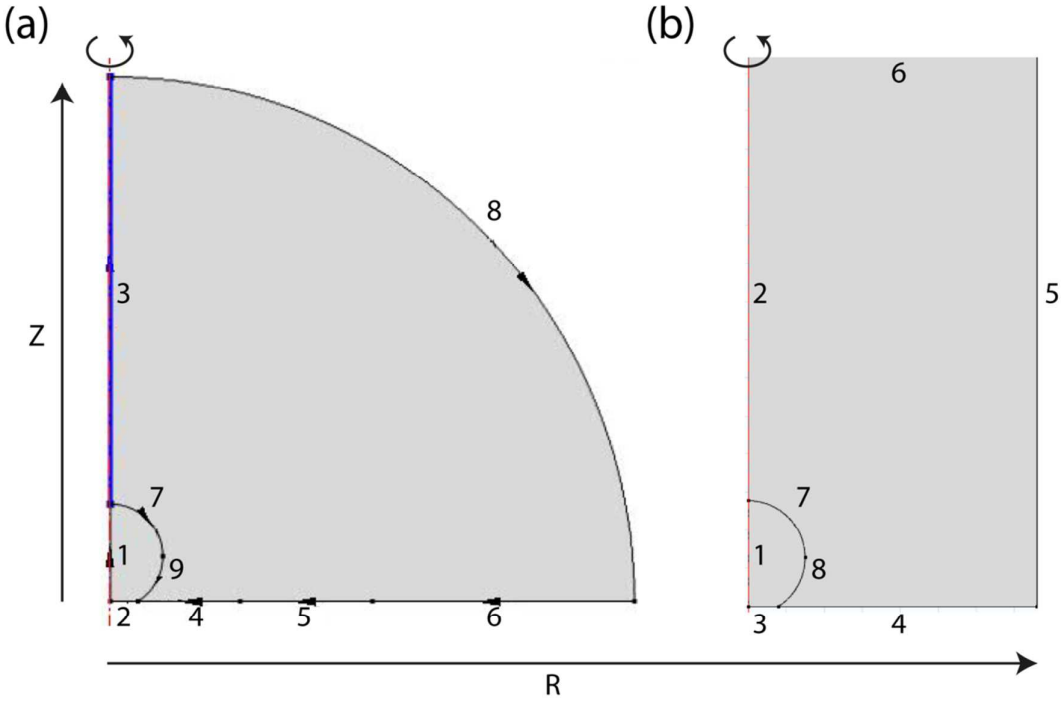

Figure 1: Simulation geometry for (a) single oil droplets on the electrode surface and (b) oil droplet arrays.

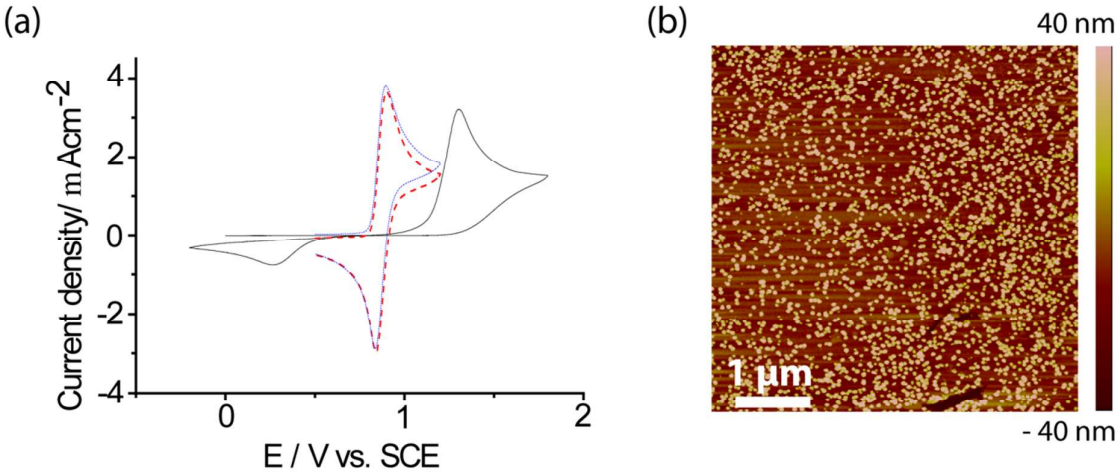

Figure 2: (a) CVs of 10 mM KBr in 0.5 M H_2SO_4, scan rate 100 mV s^{-1} at a bare 1 mm diameter disc pBDD electrode (black line), 2 mm diameter disc Pt macroelectrode (red dashed line) and a Pt NP-pBDD electrode (blue line). The currents have been normalized with respective to electrode area. (b) Tapping mode AFM image of electrodeposited Pt NPs on the pBDD electrode surface.

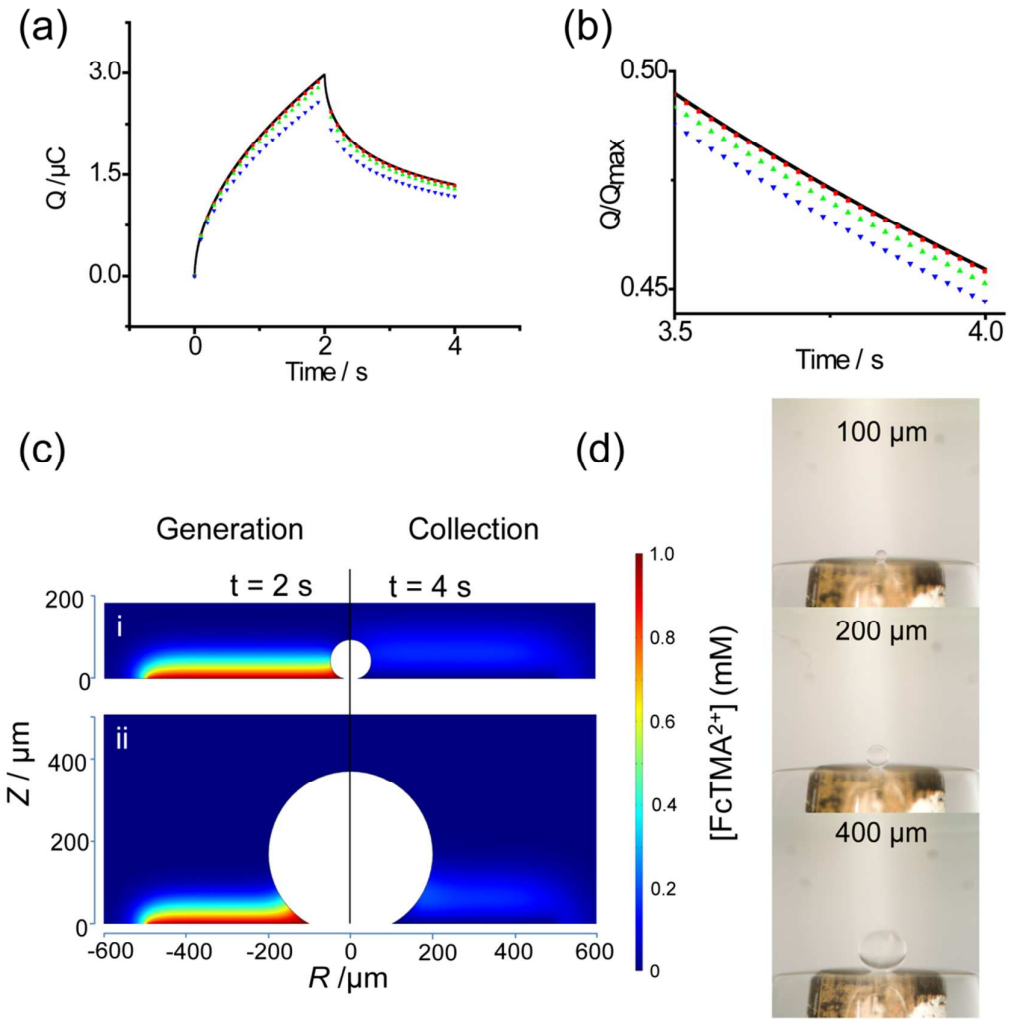

Figure 3: (a) *Q-t* plots generated from integrating the DPSC *i-t* response for 1 mM $FcTMA^+$ generation-collection at a bare Pt NP-pBDD electrode (-) and one containing a single dodecane droplet of diameter 100 μm (■), 200 μm (▲) and 400 μm (▼). (b) Plot of normalized charge (Q/Q_{max}) vs. *t* for the last 0.5 s of the collection step. (c) FEM-simulated diffusion profiles of $FcTMA^{+/2+}$ generation/collection in the presence of dodecane droplets of diameter (i) 100 μm and (ii) 400 μm diameter at times $t = 2$ s and $t = 4$ s. (d) Optical images of dodecane droplets (of diameter 100-400 μm) on a Pt NP-pBDD electrode.

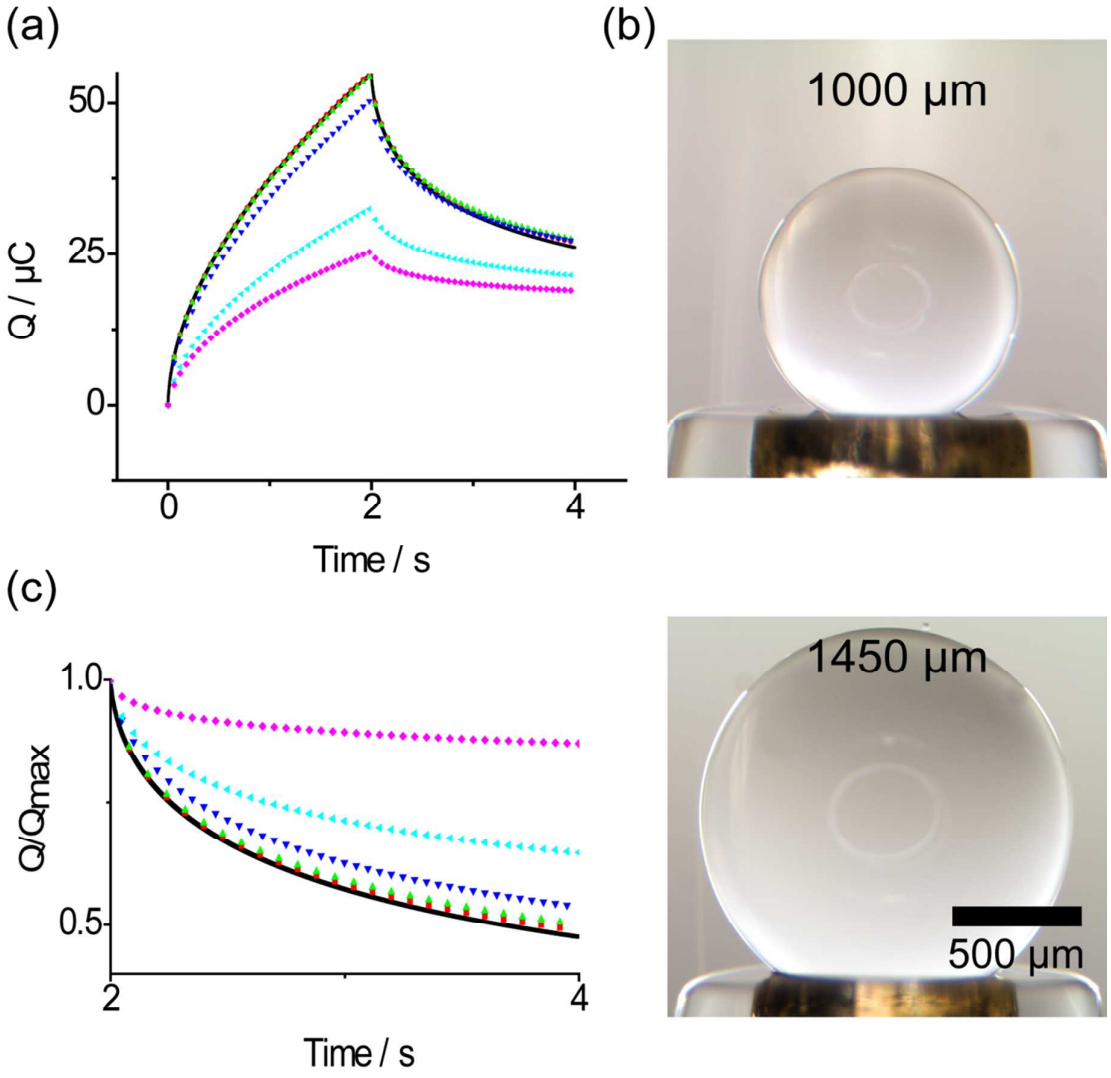

Figure 4: (a) *Q-t* plots for 1 mM Br^-/Br_2 generation-collection at a bare PtNP-pBDD electrode (-) and one containing a single dodecane droplet of diameter 100 µm (■), 200 µm (▲), 400 µm (▼), 1000 µm (◄) and 1450 µm (♦). (b) Optical images of dodecane droplets (of diameter 1000 and 1450 µm) on the PtNP-pBDD electrode. (c) Plot of normalized charge (Q/Q_{max}) vs. *t* for the collection step.

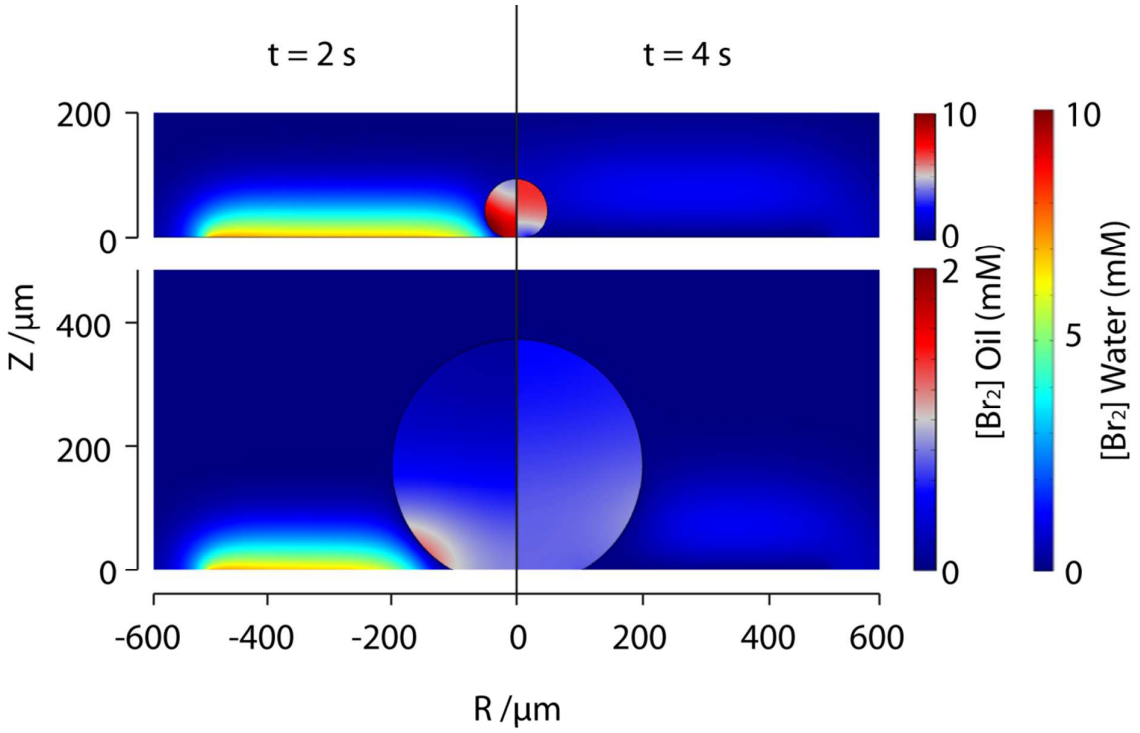

Figure 5: Diffusion profiles generated from FEM simulation of Br^-/Br_2 generation/collection in the presence of dodecane droplets (a) 100 µm and (b) 400 µm diameter at times $t = 2$ s and $t = 4$ s. Note the different scale bars for Br_2 concentration inside the oil droplet for both (a) and (b).

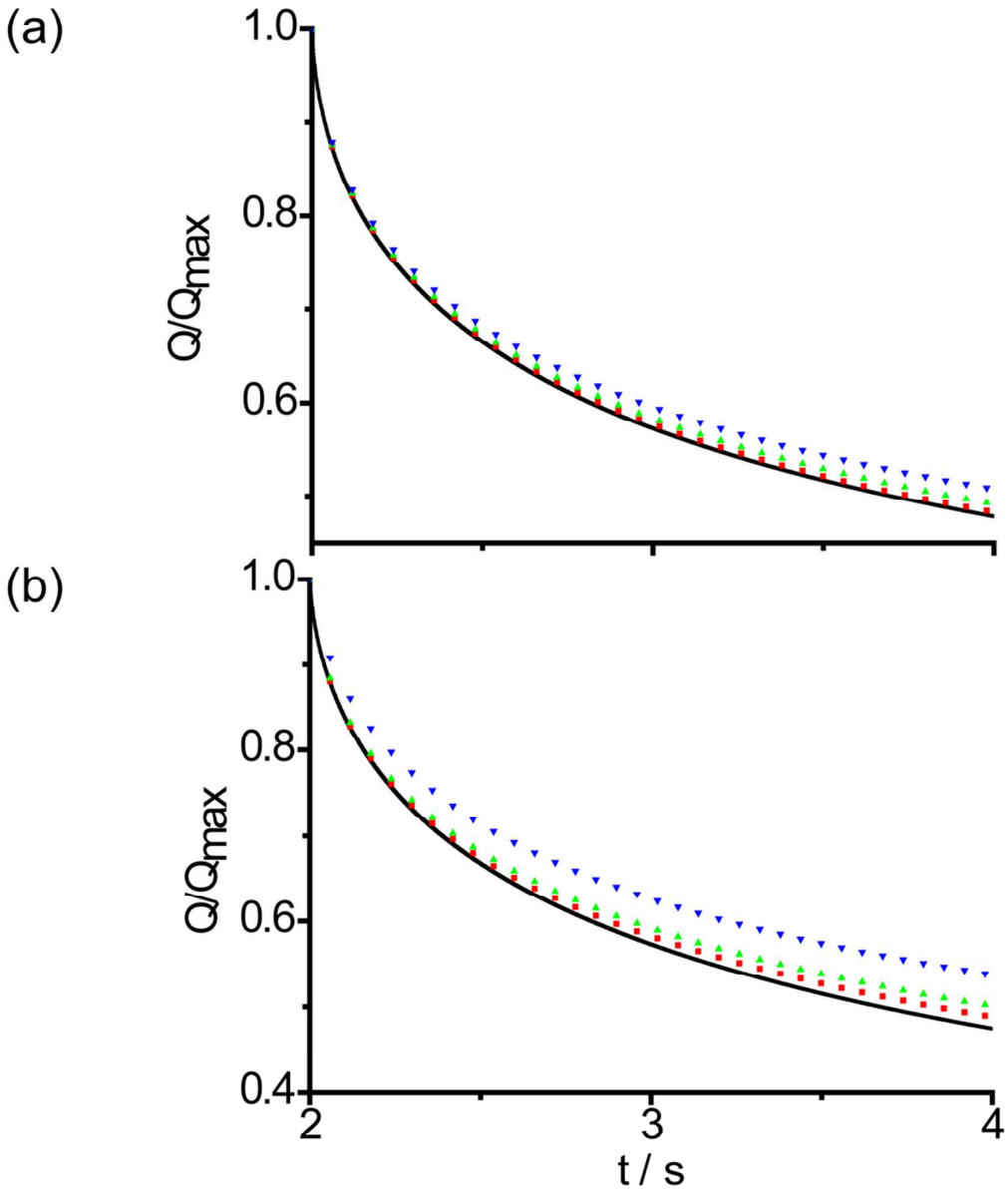

Figure 6: Plot of normalized charge (Q/Q_{max}) vs. t for the collection step i.e. collection of electrogenerated Br_2 at a bare electrode (—) and one containing a single dodecane droplet of diameter 100 µm (■), 200 µm (▲), 400 µm (▼): (a) simulated data and (b) experimental data.

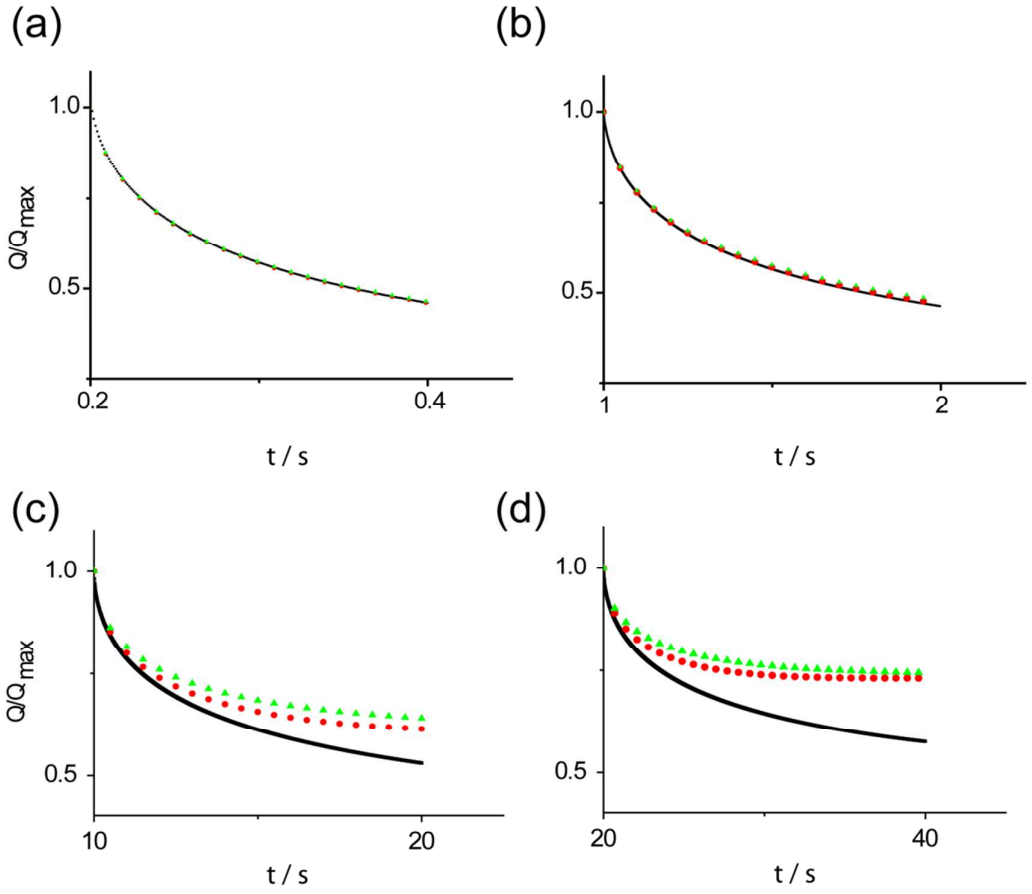

Figure 7: Normalized experimental *Q-t* plots for the DPSC Br_2 collection step with bare Pt NP-pBDD (-) and 100 µm (●) and 200 µm (▲) oil droplets present on the electrode for τ = (a) 200 ms, (b) 1 s, (c) 10 s and (d) 20 s. .

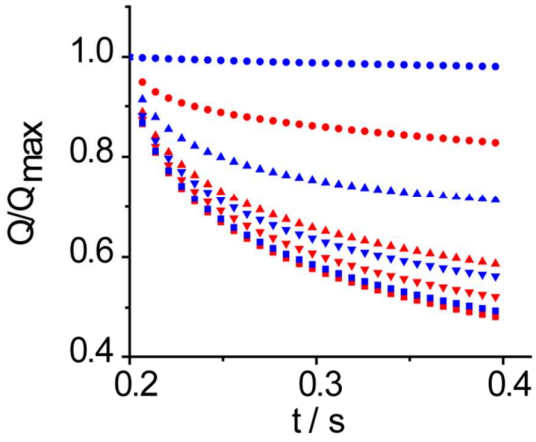

Figure 8: Plot of normalized charge (Q/Q_{max}) vs. t for the simulated collection step i.e. Br_2 collection for a PtNP - pBDD electrode of diameter 500 µm (■), 300 µm (▼), 200 µm (▲) and 100 µm (●) containing a single oil droplet of diameter 100 µm (red) and 200 µm (blue).

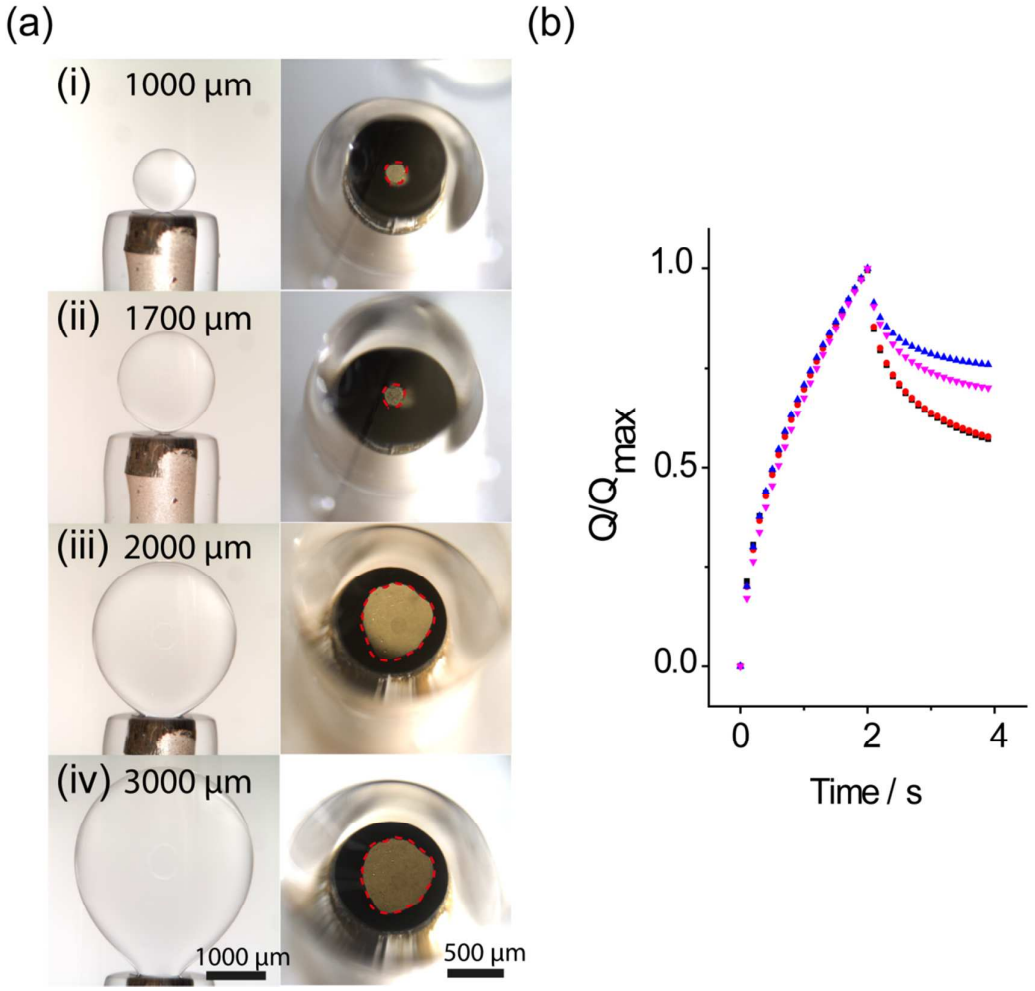

Figure 9: (a) Optical images of droplets of effective diameter (i) 1000 µm, (ii) 1700 µm, (iii) 2500 µm and (iv) 3000 µm taken side on (left hand side) and top down (right hand side). The dashed circles show the contact area of the droplet with the electrode. (b) Normalized *Q*-*t* plots for droplets of effective diameter 1000 µm (■), 1700 µm (●), 2500 µm (▲) and 3000 µm (▼).

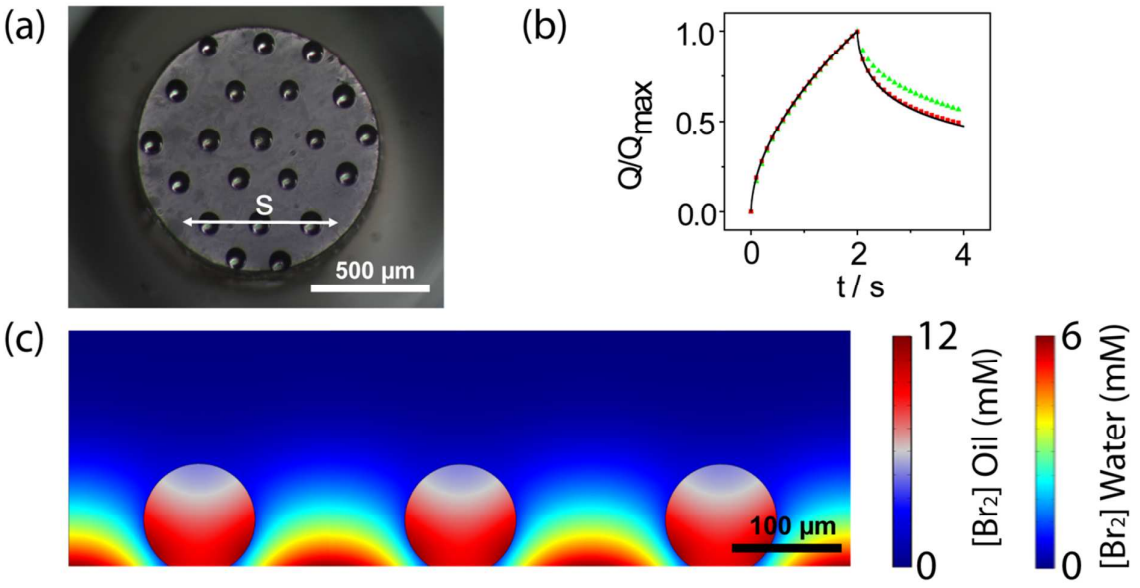

Figure 10: (a) Optical image of the oil microdroplet array on the Pt NP-pBDD electrode surface from above. (b) Normalized *Q*-t plots comparing the DPSC response of a single ~100 µm diameter droplet with a ~100 µm diameter microdroplet array (21 droplets in total). ▬ Bare electrode, ▲ ~100 µm droplet array, ■ ~100 µm droplet. (c) Diffusion profile along vector "*s*" generated by an array simulation at $t = 2$ s, multiple repeats of modelled diffusion domain stitched together.

Table of content (TOC) entry

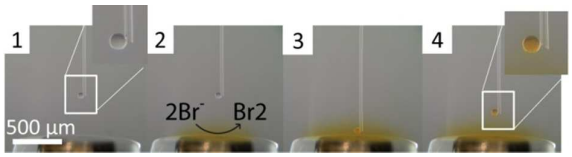

Factors affecting partitioning of an electrogenerated species, Br_2 from Br^-, into non-polar oil microdroplets at the oil-water-solid interface are investigated using double potential step chronoamperometry.

REFERENCES

1. D. W. D. Alexander G. Volkov, Darrell L. Tanelian, Vladislav S. Markin, *Liquid Interfaces in Chemistry and Biology*, John Wiley & Sons, INC, 1998.
2. D. W. D. Alexander G. Volkov, *Liquid-Liquid Interfaces Theoy and Methods*, 1 edn., CRC Press, 1996.
3. F. Reymond, H. H. Girault, G. Steyaert, P.-A. Carrupt and B. Testa, *Helv. Chim. Acta*, 1996, **79**, 101-117.
4. R. Gulaboski, A. Galland, G. Bouchard, K. Caban, A. Kretschmer, P.-A. Carrupt, Z. Stojek, H. H. Girault and F. Scholz, *J. Phys. Chem. B*, 2004, **108**, 4565-4572.
5. G. Bouchard, A. Galland, P.-A. Carrupt, R. Gulaboski, V. Mirceski, F. Scholz and H. H. Girault, *Phys. Chem. Chem. Phys.*, 2003, **5**, 3748-3751.
6. H.-S. Wu and M.-C. Lu, *J. Mol. Catal. A: Chem.*, 1995, **104**, 139-146.
7. G. D. Yadav, Y. B. Jadhav and S. Sengupta, *J. Mol. Catal. A: Chem.*, 2003, **200**, 117-129.
8. S. K. Maity, S. Sen and N. C. Pradhan, *Chem. Eng. Sci.*, 2009, **64**, 4365-4374.
9. T. Kakiuchi and H. Sasao, *Russian Journal of Electrochemistry*, 2008, **44**, 73-77.
10. Y.-T. Kong, S.-i. Imabayashi and T. Kakiuchi, *J. Am. Chem. Soc.*, 2000, **122**, 8215-8219.
11. C. Forssten, K. Kontturi, L. Murtomäki, H. C. Hailes and D. E. Williams, *Electrochem. Commun.*, 2001, **3**, 379-383.
12. F. Reymond, D. Fermín, H. J. Lee and H. H. Girault, *Electrochim. Acta*, 2000, **45**, 2647-2662.
13. F. Scholz, *Annual Reports Section "C" (Physical Chemistry)*, 2006, **102**, 43-70.
14. R. Gulaboski, V. Mirčeski and F. Scholz, *Electrochem. Commun.*, 2002, **4**, 277-283.
15. R. Gulaboski, K. Riedl and F. Scholz, *Phys. Chem. Chem. Phys.*, 2003, **5**, 1284-1289.
16. F. Scholz, R. Gulaboski and K. Caban, *Electrochem. Commun.*, 2003, **5**, 929-934.
17. F. Quentel, V. Mirčeski and M. L'Her, *J. Phys. Chem. B*, 2005, **109**, 1262-1267.
18. C. Forssten, J. Strutwolf and D. E. Williams, *Electrochem. Commun.*, 2001, **3**, 619-623.
19. X. Q. Lu, D. F. Dong, X. H. Liu, D. N. Yao, W. T. Wang and Y. M. Xu, *Chin. Chem. Lett.*, 2010, **21**, 225-228.
20. C. J. Slevin and P. R. Unwin, *Langmuir*, 1997, **13**, 4799-4803.
21. C. J. Slevin, J. Zhang and P. R. Unwin, *J. Phys. Chem. B*, 2002, **106**, 3019-3025.
22. K. Nakatani, K. Chikama, H.-B. Kim and N. Kitamura, *Chem. Phys. Lett.*, 1995, **237**, 133-136.
23. F. Marken, J. D. Watkins and A. M. Collins, *Phys. Chem. Chem. Phys.*, 2011, **13**, 10036-10047.
24. J. D. Wadhawan, A. J. Wain and R. G. Compton, *ChemPhysChem*, 2003, **4**, 1211-1215.
25. J. Wadhawan, R. Compton, F. Marken, S. Bull and S. Davies, *J. Solid State Electrochem.*, 2001, **5**, 301-305.
26. C. E. Banks, T. J. Davies, R. G. Evans, G. Hignett, A. J. Wain, N. S. Lawrence, J. D. Wadhawan, F. Marken and R. G. Compton, *Phys. Chem. Chem. Phys.*, 2003, **5**, 4053-4069.
27. A. S. Barnes, N. Fietkau, F. G. Chevallier, J. d. Campo, R. Mas, F. X. Muñoz, T. G. J. Jones and R. G. Compton, *J. Electroanal. Chem.*, 2007, **602**, 1-7.
28. N. Fietkau, F. G. Chevallier, L. Jiang, T. G. J. Jones and R. G. Compton, *ChemPhysChem*, 2006, **7**, 2162-2167.

29. C. J. Slevin, J. V. Macpherson and P. R. Unwin, *J. Phys. Chem. B*, 1997, **101**, 10851-10859.
30. J. V. Macpherson and P. R. Unwin, *Anal. Chem.*, 1997, **69**, 2063-2069.
31. I. Dumitrescu, P. R. Unwin and J. V. Macpherson, *Electrochem. Commun.*, 2009, **11**, 2081-2084.
32. H. V. Patten, K. E. Meadows, L. A. Hutton, J. G. Iacobini, D. Battistel, K. McKelvey, A. W. Colburn, M. E. Newton, J. V. Macpherson and P. R. Unwin, *Angewandte Chemie International Edition*, 2012, **51**, 7002-7006.
33. L. Hutton, M. E. Newton, P. R. Unwin and J. V. Macpherson, *Anal. Chem.*, 2008, **81**, 1023-1032.
34. L. A. Hutton, J. G. Iacobini, E. Bitziou, R. B. Channon, M. E. Newton and J. V. Macpherson, *Anal. Chem.*, 2013, **85**, 7230-7240.
35. E. Bak, M. Donten and Z. Stojek, *Electrochem. Commun.*, 2005, **7**, 483-489.
36. W. J. Albery, A. M. Couper, J. Hadgraft and C. Ryan, *J. Chem. Soc., Faraday Trans. 1*, 1974, **70**, 1124-1131.
37. R. G. Compton, G. M. Stearn, P. R. Unwin and A. J. Barwise, *J Appl Electrochem*, 1988, **18**, 657-665.
38. J. L. Conyers and H. S. White, *Anal. Chem.*, 2000, **72**, 4441-4446.
39. W. D. Cooper and R. Parsons, *Transactions of the Faraday Society*, 1970, **66**, 1698-1712.
40. J. C. Angus, Y. V. Pleskov and S. C. Eaton, in *Semiconductors and Semimetals*, eds. E. N. Christoph and R. Jürgen, Elsevier, 2004, vol. Volume 77, pp. 97-119.